Sensitivity of the Earth's magnetosphere to solar wind activity: Three-dimensional macroparticle model

S. Baraka, L. Ben-Jaffel

Sensitivity of the Earth's magnetosphere to solar wind activity: Three-dimensional macroparticle model

S. Baraka[1] and L. Ben-Jaffel[1]

Received 29 June 2006; revised 5 January 2007; accepted 15 February 2007; published 12 June 2007.

[1] A new approach is proposed to study the sensitivity of the Earth's magnetosphere to the variability of the solar wind bulk velocity. The study was carried out using a three-dimensional electromagnetic particle-in-cell code, with the microphysics interaction processes described by Maxwell and Lorentz equations, respectively, for the fields and particles. Starting with a solar wind with zero interplanetary magnetic field (IMF) impinging upon a magnetized Earth, the formation of the magnetospheric cavity and its elongation around the planet were modeled over time until a steady state structure of a magnetosphere was attained. The IMF was then added as a steady southward magnetic field. An impulsive disturbance was applied to the system by changing the bulk velocity of the solar wind to simulate a decrease in the solar wind dynamic pressure, followed by its recovery, for both zero and southward IMF. In response to an imposed drop in the solar wind drift velocity, a gap (air pocket) in the incoming solar wind plasma appeared moving toward Earth. The orientation of the cusps was highly affected by the depression of the solar wind for all orientation of IMF. The magnetotail lobes flared out with zero IMF due to the ''air pocket'' effect. With the nonzero IMF, as soon as the gap hit the initial shock of the steady magnetosphere, a reconnection between the Earth's magnetic field and the IMF was noticed at the dayside magnetopause. During the expansion phase of the system, the outer boundary of the dayside magnetopause broke up in the absence of the IMF, yet it sustained its bullet shape when a southward IMF was included. The expansion/contraction of the magnetopause nose is almost linear in the absence of the IMF but evolves nonlinearly with a southward IMF. The system recovered its initial state on the dayside soon after the impulsive disturbance was beyond Earth for both cases of zero and nonzero IMF. Comparison with existing observations from Cluster and Interball-1 seems to confirm many of our simulation results.

Citation: Baraka, S., and L. Ben-Jaffel (2007), Sensitivity of the Earth's magnetosphere to solar wind activity: Three-dimensional macroparticle model, *J. Geophys. Res.*, *112*, A06212, doi:10.1029/2006JA011946.

1. Introduction

[2] In this paper we seek to understand the general problem of the response of the Earth's magnetosphere to solar wind variability in terms of the system topology and dynamics on large scales, paying particular attention to key processes such as the magnetopause (MP) motion and the magnetic field reconnection. Our study will focus primarily on the dayside MP of the Earth's magnetosphere for which available in situ observations are quite abundant. This region was also selected because fields and plasmas in the dayside magnetosphere tend to be more ordered, and thereby make field lines mapping more tractable, and also because dayside dynamics tend to be directly driven by solar wind forcing [*Murr*, 2004].

[3] The scientific literature is rich with observations [i.e., *Hasegawa et al.*, 2006; *Haaland et al.*, 2004; *Balogh et al.*, 2001; *Bauer et al.*, 2000] and magnetohydrodynamic (MHD) calculation [i.e. *Guzdar et al.*, 2001; *Reiff and Burch*, 1985; *Lyon et al.*, 1998] pertaining to the aforementioned problem, yet these approaches are not comprehensive enough to provide an understanding of the full nature of the solar wind-Earth magnetospheric interaction, particularly at the dayside MP. In the MHD models, only ensemble-averaged parameters are available, with an assumed distribution of the particle velocity as best described by a collection of several Maxwellian functions in the most evolved version of the multifluid approximation [*Winglee et al.*, 2005]. These calculations do not determine the plasma microphysics that is specifically under the influence of the magnetic field where velocity distributions along and across the field lines are generally different. In addition, on the observational side, and for those regions near the Earth accessible to satellites, there are more limitations than the only difficulty of coverage of a large space simultaneously.

[1]Institut d'Astrophysique de Paris, UMR7095 CNRS, Université Pierre et Marie Curie, Paris, France.

0148-0227/07/2006JA011946

[4] Indeed, we face a difficult time-space problem because when satellites are moving, temporal changes cannot be distinguished from spatial variations. Further complications arise from the fact that no satellite can provide a global image of the interaction process of the solar wind with the Earth magnetosphere because in the real world, the magnetospheric macrostructure is already set when observed; therefore we cannot identify the specific interaction that shaped that structure. Moreover, in situ measurements can generally characterize the plasma only on scales smaller than the Debye length. With the launch of the NASA IMAGE satellite in March 2000, the promise of magnetospheric imaging began to materialize. IMAGE provides nearly continuous imaging of the inner magnetosphere on a nominal timescale of 2 min [*Burch*, 2005]. Simultaneous measurements of both temporal and spatial scales are rare, making it difficult to interpret the interrelationship of the two. Cluster, a set of satellites launched in 2000, is intended to fill the gap between small- and large-scale properties with simultaneous in situ observations obtained by the satellites in different regions of the magnetosphere, thereby providing a three-dimensional map (in terms of density and field configuration) of the magnetosphere. The Cluster II spacecraft has state-of-the-art plasma instrumentation to measure electric and magnetic fields, from quasi-static up to high frequency, as well as electron and ion distribution functions from around zero to a few million electron volts in energy [*Escoubet and Schmidt*, 2000]. In addition, large-scale space events of interest are infrequent and unique, and hence they do not lend themselves to general models of space plasma dynamics.

[5] Such considerations highlight the importance of our proposed computer simulation. Our approach provides a tool that spans all boundary conditions instantaneously and globally while keeping track of the plasma physics locally on a selected scale (here the planet radius). Because at each unit time of the code we access the microphysics of the plasma at the considered length scale, this method reveals details of the magnetosphere well beyond the limitations of the existing three-dimensional MHD methods and the local imaging by orbiting satellites of certain areas of the magnetosphere.

[6] In the past, several versions of the TRISTAN code had been developed, which were successful in recovering the main features of the Earth's magnetosphere [*Nishikawa*, 1997; *Wodnicka*, 2001; *Cai et al.*, 2006]. In this study, we use an updated version of the code that more accurately handles instabilities and at the same time reduces CPU time (*L. Ben-Jaffel et al.*, in preparation, 2006). In the first step, we consider a simulation box of reduced dimensions intended to validate our simulation code through a comparison to standard magnetosphere structures gathered from observations over the last decades. In the following step, the simulation box is enlarged with a finer grid that is intended to improve the accuracy of the response of the Earth's magnetosphere to a compression or depression in the solar wind although it must be kept in mind that the highly variable nature of the solar wind may produce features on small scales. To enhance our view of the interaction process, we undertook a study of the impact of the interplanetary magnetic field (IMF) on the solar wind forcing of the magnetosphere. In all cases, the MP variation in three-dimensional and the related components of momentum, local densities, and magnetic fields were recorded and studied. The time relaxation was then derived for the MP after the system was restored to its initial state in both cases, respectively, with and without the presence of the IMF. Final conclusions are then proposed regarding the benefit of using PIC simulations to understand the magnetosphere's response to a simple pressure forcing, to make predictions, and to build diagnostic tools that could be useful for future comparison to data.

2. Code Description

[7] To perform our simulations, we use a particle-in-cell (PIC) code first developed by *Buneman* [1993]. This code is a fully three-dimensional electromagnetic and relativistic code. In our model, the magnetosphere is sketched as an ensemble of macroparticles: macro-ions and macro-electrons. Motions of these macroparticles are simulated in three-dimensional perspective under the influence of electric and magnetic fields through the Lorentz law. The fields themselves are described by Maxwell's equations. Because of its construction, the code offers the advantage of containing the complete physics of the problem. However, the price to be paid is that we must scale some of the plasma parameters in order to perform the simulations in realistic computing times. The complexity and limitation of the code as it was initially written made it difficult to access and limited its applications to a few case studies. In other words, the difficulties are in establishing good resolution in time and space and limitation with a smaller m_e/m_i mass ratio. However, this method is superior to MHD simulations in some aspects such as in modeling kinetic processes that separate the electrons and ion dynamics [*Nishikawa*, 1997; *Wodnicka*, 2001; *Cai et al.*, 2006]. We are using a modified version of the code in terms of numerical stability, computer CPU time, and consistency with the real world, a version developed in collaboration between the Institut d'Astrophysique de Paris and the Space Research Center of Poland (*L. Ben-Jaffel et al.*, in preparation, 2006).

[8] In our simulation, we applied radiating boundary conditions for the fields as proposed by *Lindman* [1975]. At the boundary, macroparticles are annihilated. The trajectories of ions and electrons are computed, solving the Lorentz equation of motion [*Boris*, 1970]. Fields are updated using Maxwell's equations. A charge conservation argument is applied, following the formulas of *Villasenor and Buneman* [1992]. The plasma was initially neutral and characterized by an isotropic Maxwellian velocity distribution. The solar wind bulk velocity and the electron-to-proton mass ratio are the basic controlling parameters in the code. These two parameters are scaled so that the main features of the Earth's magnetosphere, such as the MP standoff distance, are recovered for a reference solar activity. This scaling offers the benefit of significantly reducing the computer CPU time while keeping track of the main physical processes, such as separating the dynamics of electrons and ions instantaneously [*Buneman*, 1993; *Nishikawa et al.*, 1995]. While our code may generate any field orientation, a zero dipole tilt is assumed for the sake of simplicity. The dipole magnetic field was initially set to zero and was then switched on. The IMF along the z axis was included,

and the corresponding electric field along the y axis was generated assuming a frozen-in condition for the solar wind flow.

[9] The code parameters in this study adopt many of those proposed by *Nishikawa* [1997, 1998], *Nishikawa and Ohtani* [2000], and *Cai et al.* [2006]. Our grid size is $\Delta = 1$ R_e, and $\Delta t = 1$ unit time, where $\Delta = \Delta x = \Delta y = \Delta z$. In our model, for the code validation stage, our simulation box is the size $(x, y, z) = (105\Delta, 55\Delta, 55\Delta)$, the Earth's position is located at $(x, y, z) = (40\Delta, 27\Delta, 28\Delta)$, and the box is filled with 5×10^5 electron-ion pairs. For other cases studied, this size is enlarged to $(x, y, z) = (155\Delta, 105\Delta, 105\Delta)$, loaded with 2×10^6 electron-ion pairs, and the Earth's position is located at $(x, y, z) = (60\Delta, 52\Delta, 53\Delta)$. The plasma parameters in our code are summarized as follows: the solar wind drift velocity is set to $0.5c$ ($c = 0.5$ being the speed of light in the code), applied along the x direction at time range $0 < t < 1000\ \Delta t$ during the code validation case. In our study cases, the code was initially run up to $900\ \Delta t$ to build up the classical structure of the magnetosphere before applying any perturbation on the system. It is worth noting that the solar wind number density input is held constant over all the cases studied.

[10] Our real time has been rescaled in the code based on the Courant condition, which states that during the simulation, the time step must be less than the time for some instabilities to grow and, preferably, considerably less [*Matsumoto and Omura*, 1993]. From the Courant condition $c\Delta t \leq \frac{\Delta r}{\sqrt{3}}$, where the real values of the solar wind velocity and the Earth's radius are $v_{sw} = 500$ km/s and $R_e = 6335$ km, respectively. The injected solar wind density is 0.8 electron-proton pairs per cell ($0.8/\Delta^3$), and the mass ratio is $m_e/m_i = 1/16$. After scaling, the thermal velocity is $v_{th_{e,i}} = (0.1, 0.025)$, the plasma frequency is $\omega_{e,i} = (0.89, 0.22)$, and the Debye length $\lambda_{De,i} = (0.1, 0.1)$, where "e" and "i" denote electrons and ions, respectively.

[11] It may be worth noting to remark that the way the PIC code was built is to have the fields evaluated over the grid nodes, while particles can have any position within the box. Kinetic effects of particles are then included, although fields are averaged over a cell's scale (1 R_e here), and the particle mass ratio, m_i/m_e, is large but far from its real value. It follows that our PIC code is well designed for the study of the macrostructure of a magnetosphere but requires a denser grid and a better particle statistics for smaller scales [*Cai et al.*, 2006].

3. Results

[12] To study the sensitivity of the Earth's magnetosphere to the variability of solar wind bulk velocity, the first step is to build a steady state magnetosphere. Using the PIC code described in the previous section, we proceed with a simulation box of dimensions $(155, 105, 105)\Delta$, loaded with 2×10^6 electron-ion pairs, where Earth is located at $(60, 52, 53)\Delta$. The code was first tested for a smaller box of size $(105, 55, 55)\Delta$ and less solar wind electron-ion pairs 5×10^5 to check its validity and to build reference models to analyze more complicated cases with a variable incident solar wind. For that purpose, three simple test cases of slow, moderate, and fast solar wind velocities were studied and are presented in section 3.1. In section 3.2, in order to study the effect on the Earth's magnetosphere of an "air pocket" in the solar wind flow, we compute models with a sudden drop in the ram pressure of the solar wind, both with and without the presence of the IMF. Such pressure variations (depression) have never been considered in previous studies although the occurrence of such events in nature should be common.

3.1. Test of the Code and Reference Models

[13] We start with the first case where a zero dynamic pressure (i.e., $V_{sw} = 0.0$) of the incident solar wind flow is applied. Initially, the geomagnetic field is set to zero, and the box is filled with pairs of macro-ions/macro-electrons so that a plasma density of $0.8/\Delta^3$ is obtained. Inside the box, the particles have a bulk velocity of 0.25 in addition to the thermal component that corresponds to each species. As the incident solar wind bulk flow is set to zero outside the box, obviously, no more particles feed the simulation box unless by thermal motion. The Earth's magnetosphere in the noon-midnight plane (x-z plane at $y = 27\Delta$) is shown in Figure 1. The plasma density is given in panels A and B, and their corresponding fields are shown in panels C and D, respectively, at 100 and $1000\ \Delta t$. The initial density of $0.8/\Delta^3$ is a statistical average which is consistent with larger peak density values as indicated by the color bar. First, we note the symmetry between day- and nightsides in the plasma density configuration around the planet. It is significant that the code recovers the dipole nature of the planetary field with little effect from the initial plasma dynamic pressure inside the simulation box (Figure 1C). In Figure 1B, taken at $1000\ \Delta t$, the magnetosphere structure clearly appears despite the absence of external plasma sources and the continuing loss of particles from the box. For the sake of clarity, we recall that our initial conditions are such that the simulation box was initially filled with pairs of electron-ions that have a bulk velocity of 0.25, but no new incident solar wind particles are injected in the box. As a consequence, the system is loosing particles with time, and this explains the magnetospheric structure obtained in Figure 1B. In addition, we notice a clear entering of plasma from the polar cusp and repopulation of the equatorial plasma sheath at the nightside.

[14] In Figure 1C, we notice the symmetry of the field lines around the planet although the system is still in an evolution phase. Figure 1D shows that the field lines are slightly elongated tailward and mimic the plasma distribution shown in Figure 1B. The topology of these field lines resembles a dipole-like shape although a bit squeezed on the dayside and elongated at the nightside. To some extent, the results so far obtained with this first test confirm the power of the PIC code and legitimize the use of the macroparticle model to describe the magnetospheric structure on large scales.

[15] In the following step, the incident solar wind drift velocity (V_{sw}) is increased to a moderate value of 0.1 while keeping the box initially filled with particles that have a bulk velocity of 0.25. Figure 2 contains four panels: A and B show the density distribution at 100 and $1000\ \Delta t$, respectively, while C and D show the fields at the same time periods. In Figure 2A, at an early stage of the interaction taken at $100\ \Delta t$, a clear modification has taken place in the configuration of the magnetosphere symmetry

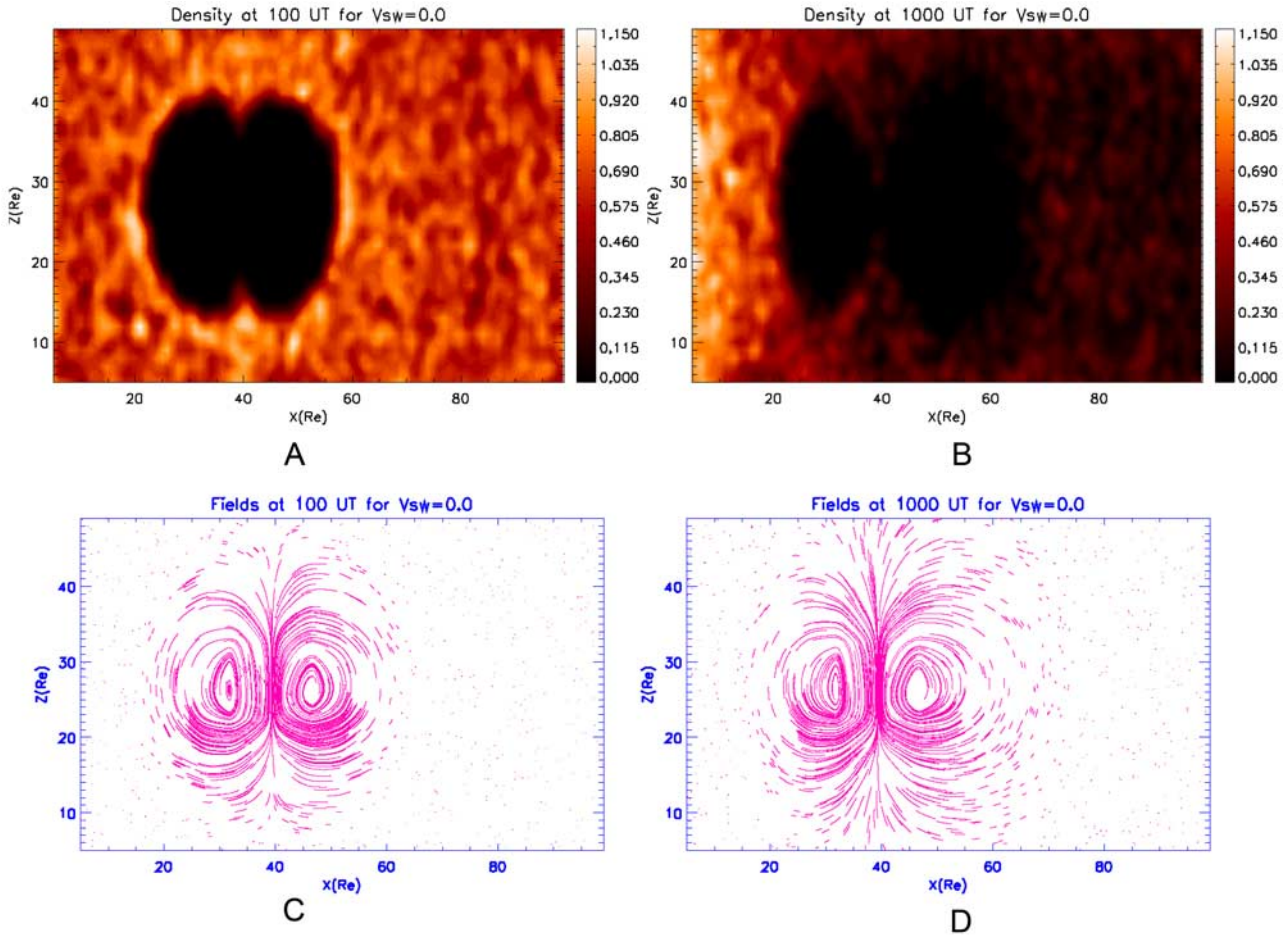

Figure 1. Earth's magnetosphere formation inside a box filled by e-ion pairs that have a bulk velocity of 0.25. Solar wind particles incident on the left side of the box have their bulk velocity $V_{sw} = 0.0$. All plots are in the x-z plane located at $y = 27\ R_e$. Plasma distribution is shown in panels A and B, taken at 100 and 1000 Δt, respectively. The corresponding field topology is shown in panels C and D, taken at 100 and 1000 Δt, respectively.

as compared to the results obtained in the previous step with $V_{sw} = 0.0$. The compression of the magnetopause at the dayside is accompanied by a relaxation on the nightside.

[16] Figure 2B clearly reveals a significantly compressed magnetopause nose, with the cusps-plasmas entering into the Earth's magnetosphere from both poles. The nightside plasma configuration is quite stretched and elongated. From 80 to 100 R_e along the x axis, the formation of blobs of plasma in the equatorial plane (at $z = 53\ R_e$) and along the neutral line is clearly seen. In Figure 2C, taken at 100 Δt ($\sim$300 s), the field lines show the modification of the system due to the increased ram pressure of the incident solar wind, particularly on the dayside. Figure 2D, taken at 1000 Δt, shows how the dayside field lines are compressed inward, while on the nightside, the field lines are stretched away and straightened tailward, much like the plasma distribution. Field lines clearly flare out at the early nightside, and the cusps are clearly seen in the field topology.

[17] To refine our testing of the code, the solar wind drift velocity is now modified to a stronger value of 0.25. As in the previous cases, in Figure 3, panels A and B show the density distribution at 100 Δt ($\sim$300 s) and 1000 Δt ($\sim$3000 s), respectively, while panels C and D show their corresponding distributions of the fields.

[18] In Figure 3A, the magnetospheric cavity is not yet established (compare to Figure 3B) with a noticeable compression on the dayside because of the increase in the ram pressure of the incoming solar wind, but the polar cusps are clearly seen. In Figure 3C, the field topology, corresponding to the plasma distribution shown in panel A, shows the compression of the field lines at the nose. At approximately 67 R_e on the nightside, opened field lines are clearly seen with the beginning of the tail formation.

[19] Figure 3B reveals that the so-called trapping region around the equatorial plane now seems thicker (thickness $\sim 5.3\Delta$). The plasma sources in that region are expected from both the cusps and the plasma driven from the nightside through the neutral line. We soon observe a clear formation of plasma clouds (i.e., random-shaped ensembles of plasma) at around $80-100\Delta$. We mean by plasma clouds the low-density random-shaped ensembles of plasmas. Figure 3D shows the field line topology corresponding to the plasma in panel B. On the nightside, field lines are straightened and stretched out tailward. At around 73 R_e, we see an x point. On the former right-hand side, the field lines

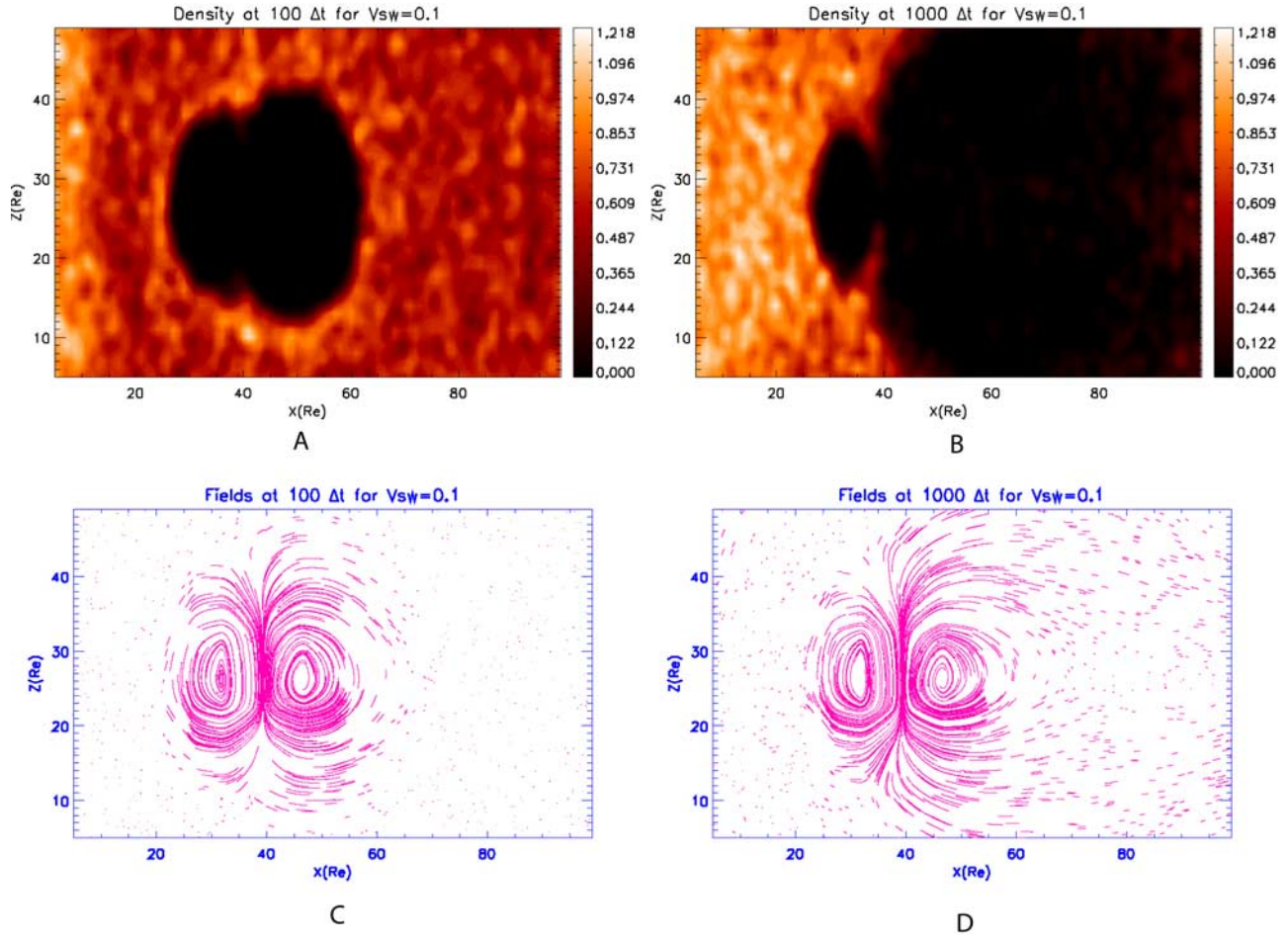

Figure 2. Earth's magnetosphere formation inside a box filled by e-ion pairs that have a bulk velocity of 0.25. Solar wind particles incident on the left side of the box have their bulk velocity $V_{sw} = 0.1$. All plots are in the x-z plane located at $y = 27\ R_e$. Plasma distribution is shown in panels A and B, taken at 100 and 1000 Δt, respectively. The corresponding field topology is shown in panels C and D, taken at 100 and 1000 Δt, respectively.

form a vortex-like structure, centered at the point $(x, z) = (88, 20)R_e$, which corresponds to the plasma spherical clouds that were seen on the tail side in panel B. It is interesting to note that the equatorial plasma sheet is well developed and has a variable thickness that may reach a few R_e.

[20] After analyzing these cases, we conclude that our PIC code recovers what is known about the large structure of the Earth's magnetosphere for all regimes of solar wind ram pressure. Hence the next set of tests for our code is designed to check its capacity to simulate the time variability of the magnetosphere on selected timescales. For example, one of the most manifest natures of solar wind is its dynamic pressure variability, which we choose to simulate. Depression/compression of the solar wind is simulated by applying abrupt changes to the speed of the steady flow of the solar wind particles inside the simulation box.

[21] Shown in Figure 4, in the noon-midnight plane, is a steady flow of solar wind particles, with a bulk velocity of 0.25, which have been injected into the simulation box. The process enables the system to evolve up to 400 Δt, thereby allowing enough time to establish the classical macrostructure of the Earth's magnetosphere. Next, the solar wind bulk velocity is reduced to 0.1 for 100 Δt. At 500 Δt, V_{sw} is again increased to its initial value of 0.25, and the process continues until 1000 Δt. As a result, a gap is generated in the incident plasma structure that can be defined by the drop in both the bulk velocity and the plasma density along the x axis. This structure results in response to the sudden drop in plasma dynamic pressure. The upstream boundary of the formed gap is around 13 R_e and moves with the initial steady state speed of 0.25, while the one downstream is around 28 R_e. As shown, the gap has a width of approximately 15 R_e, which is consistent with the picture of a differential speed applied during 100 Δt, for example, $(0.25-0.1) \times 100 = 15\ R_e$. Our code, then, is capable of reproducing pulse events in the solar wind properties and following them with time while measuring their impact on the magnetosphere. Such will be the purpose of the following section that utilizes a finer grid.

3.2. Study of the Impact of a Solar Wind Depression Event on the Earth's Magnetosphere

[22] In order to deepen our understanding of the magnetospheric response to a sudden change in the solar wind

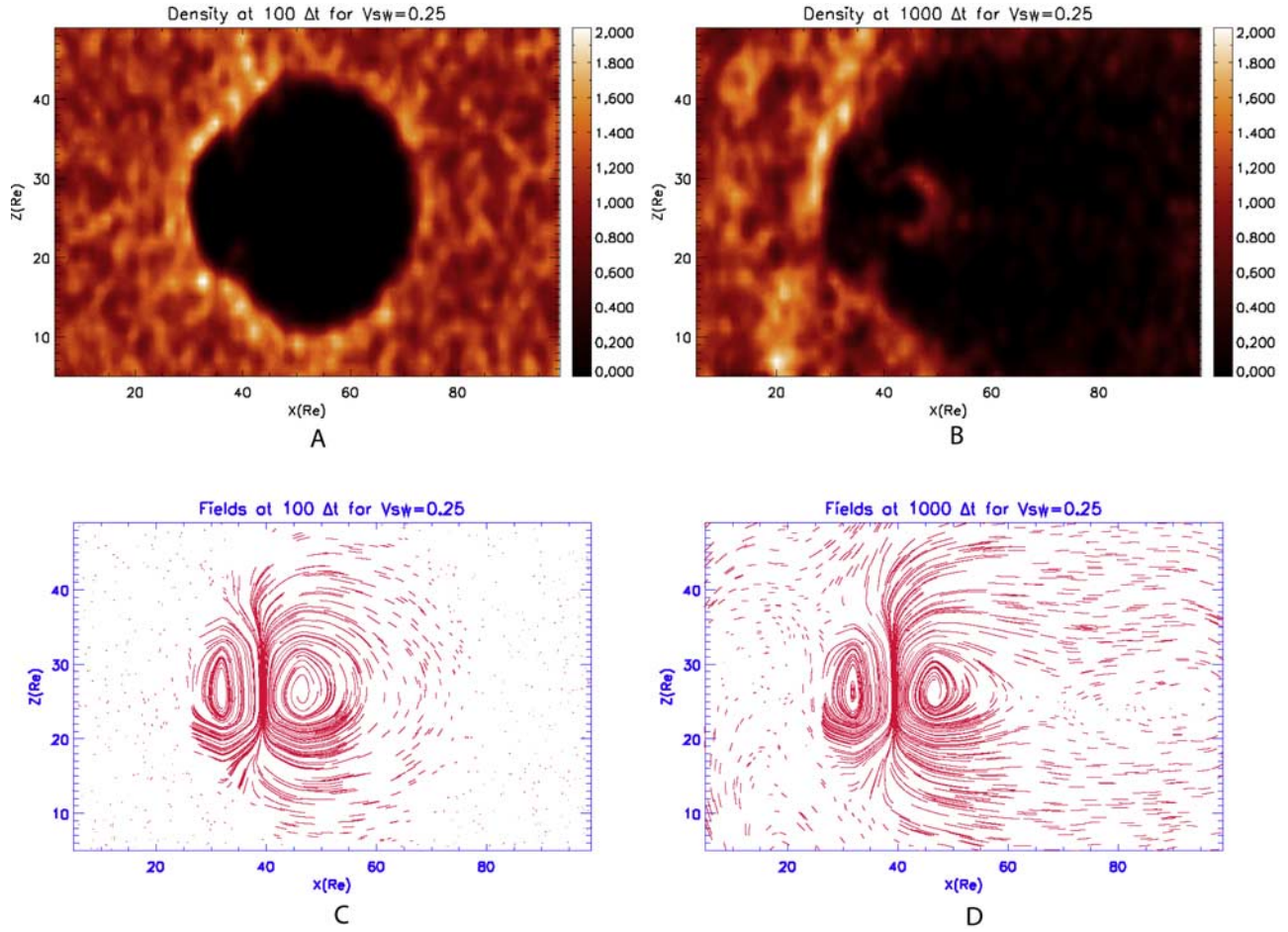

Figure 3. Earth's magnetosphere formation inside a box filled by e-ion pairs that have a bulk velocity of 0.25. Solar wind particles incident on the left side of the box have their bulk velocity $V_{sw} = 0.25$. All plots are in the x-z plane located at $y = 27$ Re. Plasma distribution is shown in panels A and B, taken at 100 and 1000 Δt, respectively. The corresponding field topology is shown in panels C and D, taken at 100 and 1000 Δt, respectively.

velocity, we extend the simulation box dimension to $(x, y, z) = (155\Delta, 105\Delta, 105\Delta)$, which is now initially loaded with 2×10^6 electron-ion pairs. Our images also trim 5 R_e from each boundary corresponding to the buffer of our simulation box for both plasmas and field representations to avoid any edge effect. Because our graphics software uses random numbers to draw contours, the final visual output is rather difficult to control, particularly for field lines. Therefore we reduce the density of stream lines per plot in order to avoid image saturation and production of artificial features.

[23] In the following, two case studies are considered. First, we present the results of the interaction of the solar wind with Earth magnetosphere when there is no IMF ($B_z = 0$). Next, in the second case, we present the results when a southward pointing IMF ($B_z < 0$) is included.

[24] In the first case, when $B_z = 0$, we first obtain a steady state by simulating the interaction process between the solar wind dynamic pressure and the Earth's magnetosphere up to 900 Δt; we then reduce V_{sw} from 0.25 to 0.1, and, accordingly, the ram pressure drops by 60% of its initial value during 100 Δt before being restored to its initial value. Consequently, a moving gap formed, as shown in Figure 5a, when the former was located at positions

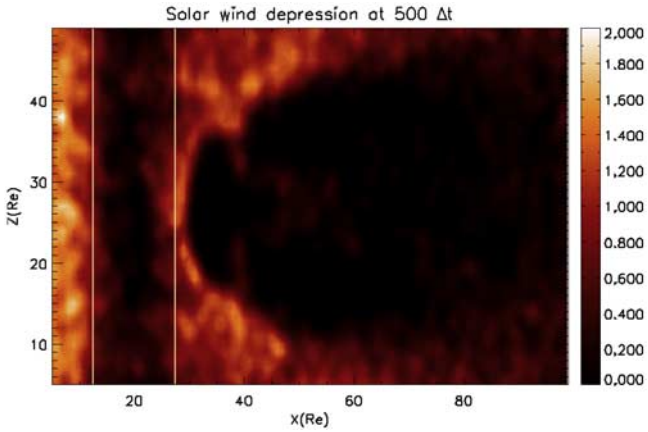

Figure 4. Gap generation due to a depression in the solar wind flow during its interaction with Earth's magnetosphere at step time 500, plotted in x-z plane located at $y = 27$ R_e. At the selected step time, the gap is centered at $\sim 20\Delta$ along the x axis and is shown between the two vertical parallel bars. It has a width of $\sim 15\Delta$.

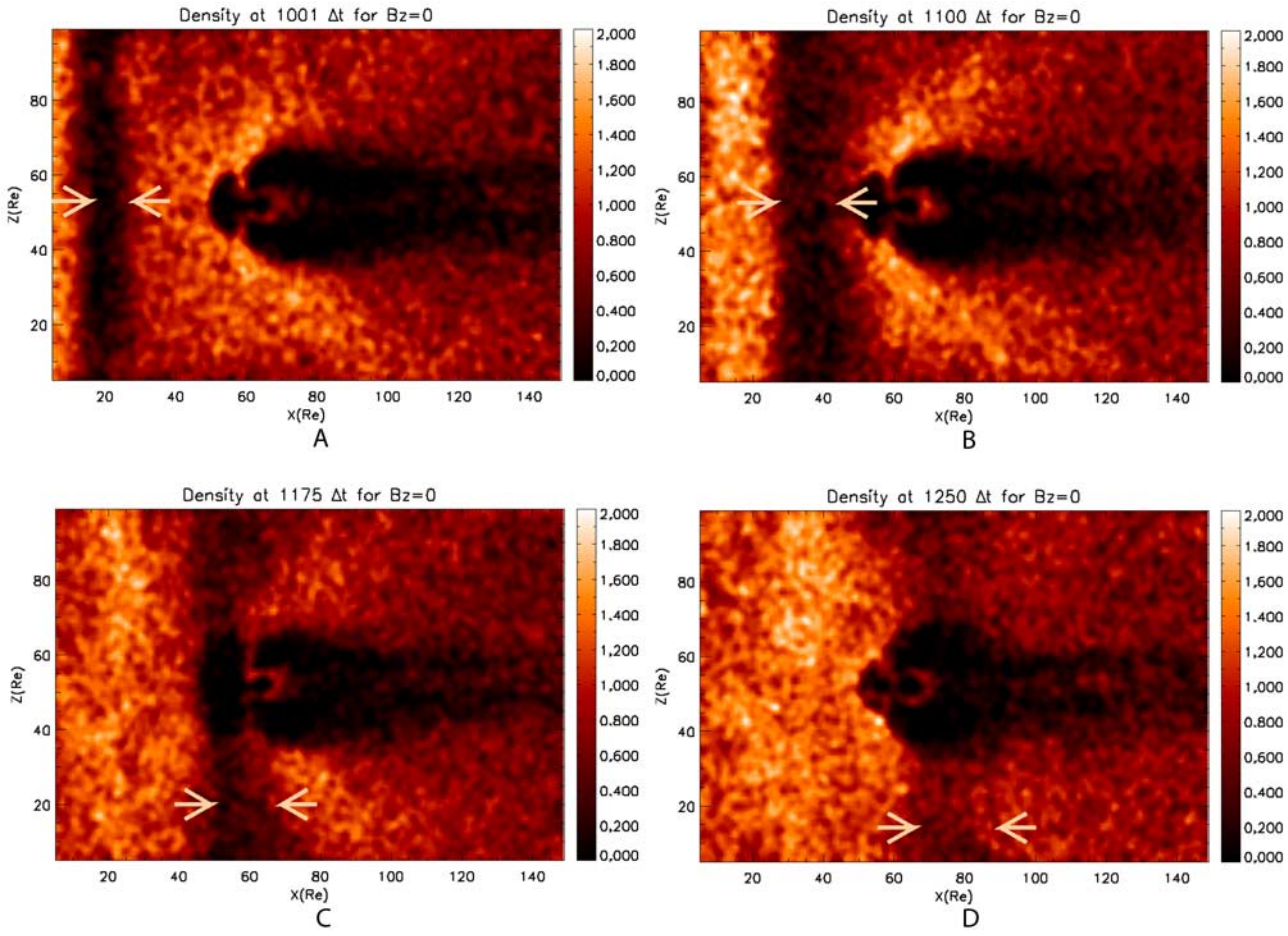

Figure 5a. Time sequence of the response of Earth's magnetosphere to a depression (air pocket effect) in the incident solar wind flow for $B_z = 0$. Plasma density is shown in panels A, B, C, and D, taken at 1001, 1100, 1175 and 1250 Δt, respectively. All plots are shown in the x-z plane located at $y = 52$ R_e, and the gap position along x direction is shown in figure between the two arrowheads.

between 12 and 27 R_e along the Sun-Earth line at time step 1001. Clouds of plasma from the tail fill the formed cavity and feed the equatorial plane with a plasma sheet that has a variable thickness. The plasma sheet mentioned here is a planar plasma distribution along the neutral line that can be seen between (x, z) = (80, 45) R_e and (120, 50) R_e. The cusps are clearly visible. As expected, the particles entering the cusp bounce back and forth due to the exchange of the parallel plasma velocities for the perpendicular velocities, thereby producing the magnetic mirror effect as evidenced by following the particles' motion with time in that region.

[25] In Figure 5a, taken at 1100 Δt, the downstream boundary of the generated gap reaches the dayside magnetopause. At that time, the expansion of the magnetopause apparently extends to 13.5 R_e along x axis. Within the gap, light clouds of plasma of random distribution are seen, some of which reverse direction toward the Sun (in the next section, we detail this reversal of velocity). On the tail side, a stream of plasma sheet replenishes the space along the neutral line. Figure 5b reveals a new situation where the magnetopause surface (nose), after an expansion period, breaks up within the gap. During the expansion phase, the stretched magnetopause appears as a thin, distorted layer that breaks up at a distance of approximately 15.5 R_e from Earth at ~1132 Δt. Soon afterward, the extended magnetopause boundary hits the upstream boundary of the gap area. Plasma clouds (blobs) are visible in the extended dayside cavity of the magnetosphere. The orientation of the cusps (seen as almost upright in this case) is highly affected by the travel of the solar wind depression inside the system. A relatively large plasma cloud is observed along the neutral line at about ~80 R_e tail side.

[26] Figure 5b shows that after the solar wind gap boundaries pass over the dayside magnetopause, the latter has restored its classical shape with a nose position at approximately 10 R_e from Earth. A thin ring of plasma corresponding to the noon-midnight section of the trapping region is formed around the planet. The size of this region reaches 6.6 R_e at the nightside equatorial plane. The shape and orientation of the cusps are highly susceptible to changes induced by the gap travelling through the system. At the early nightside, we notice that the magnetospheric structure flared out despite the fact that $B_z = 0$. We believe that the lobes respond positively to the drop in the ram pressure when the gap approaches them, and, as a result, they stretch out. Therefore this flare-out is due to the drop in the solar wind pressure rather than the interplanetary magnetic field. At 100–145 R_e, lobes are parallel to the Sun-

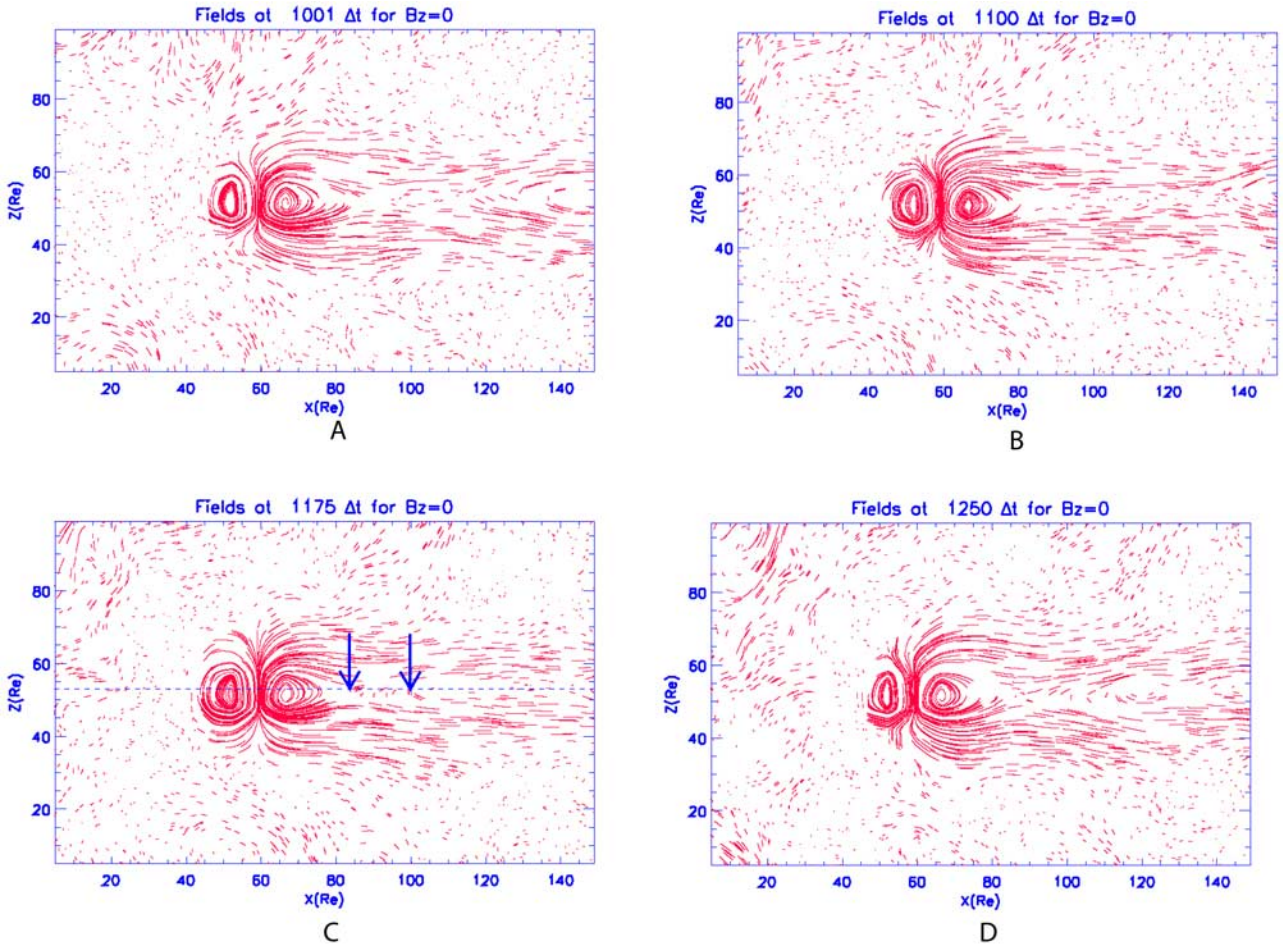

Figure 5b. Time sequence of the response of Earth's magnetosphere to a depression (air pocket effect) in the incident solar wind flow for $B_z = 0$. Field lines are shown in panels A, B, C, and D, taken at 1001, 1100, 1175, and 1250 Δt, respectively. All plots are shown in the x-z plane located at $y = 52\ R_e$.

Earth line, with large plasma clouds formed around the equatorial line.

[27] In terms of field line topology in the x-z plane, we see in Figure 5a, taken at 1001 Δt, that the dayside magnetopause stands at around 10.3 R_e from Earth along the Earth-Sun line. The lobes are seen as approximately parallel to the Sun-Earth lineup to this time because the gap effect is not yet felt by the nightside system. An x point can be seen at 103 R_e. The configuration of the field lines at the tail side implies the existence of plasma concentrated in that region centered at the point $(x, z) = (140, 47)\ R_e$. In Figure 5a, taken at 1100 Δt, the magnetopause nose is seen expanded up to 15 R_e from Earth. The field line topology is clearly seen driven tailward. At around $x = 140\ R_e$, a vortex-like configuration of the field lines denotes the plasma confined at that distance as shown by Figure 5.

[28] Figure 5b, taken at 1175 Δt, illustrates how the field lines at the dayside magnetopause start breaking up at around 15.48 R_e from Earth. Open field lines are clearly seen around this distance, and this field configuration corresponds to the plasma distribution shown in Figure 5b. One also sees the x point at 103 R_e. Field line configurations at the nightside up to 100 R_e have a wavy shape, much like their corresponding plasma in that region. This configuration corresponds to the interaction between the plasma seen at 80 R_e (for example, Figure 5a) and the plasma traveling earthward from the far tail. In Figure 5b, taken at 1250 Δt, the magnetopause nose position reads the value of 10.30 R_e from Earth: This means that it has been recovered after the depression effect is over in the dayside magnetopause. The topology of the field lines shows vortex-like (confined) structures that may be single or multiple along the neutral line (at $x = 120\ R_e$, and 145 R_e for $z = 53\ R_e$). For example, one may count up to 4 such vortex-like structures during the time evolution of the system. The gap position now is approximately between 65 and 85 R_e along the x axis (see Figure 5b), which results in stretching of the lobes and thus pulling the position of the x point earthward, now seen at $(x, z) \sim (90, 53)\ R_e$.

[29] In a second study, we present the results of the interaction of a solar wind "air pocket" with Earth's magnetosphere when IMF is included as a steady southward field ($B_z < 0$). As in the previous case, the system is first allowed to become established before the depression takes place at 900 Δt; V_{sw} is then reduced from 0.25 to 0.1, and, accordingly, the ram pressure drops by 60% of its initial value during 100 Δt before being restored to its initial value (see Figure 6a, taken at 1001 Δt). This effect results in the

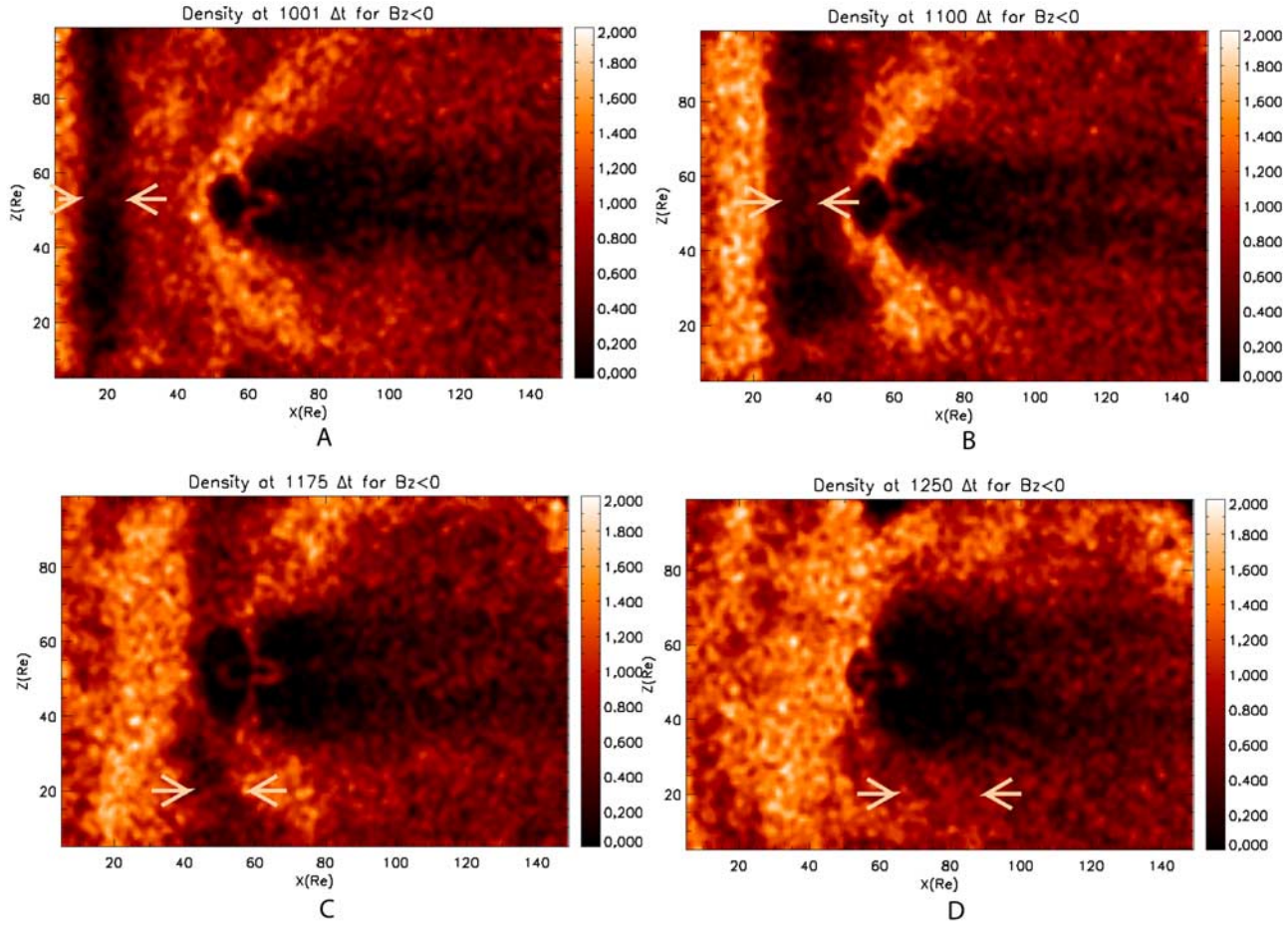

Figure 6a. Time sequence of the response of Earth's magnetosphere to a depression (air pocket effect) in the incident solar wind flow for $B_z < 0$. Plasma density is shown in panels A, B, C, and D, taken at 1001, 1100, 1175 and 1250 Δt, respectively. All plots are shown in the x-z plane located at $y = 52\ R_e$, and the gap position along x direction is shown in figure between the two arrowheads.

formation of a 15-R_e wide gap located between 10 and 25 R_e along the x axis as shown in Figure 6a. The classical structure of the Earth's magnetosphere is easily observed, and one can see the signature of the Earth's bow shock at 44–48 R_e. The cusps are quite prominent and nightward-oriented. In panel B, taken at 1100 Δt, an expansion of the magnetopause sunward is noticed due to the depression ahead of the nose. The bow shock can be seen at around ~48 R_e along the x axis. As the gap moves downstream earthward, it begins to show a curvature around 5–20 and 80–100 R_e along the z axis that appears as a departure from the z direction toward the planet. This curvature is the result of the boundary of the gap that begins to respond to the strong magnetic pressure of the Earth on the Sun-Earth symmetry line, while across, at both ends of the boundary along Oz, this pressure is not yet fully felt, and thus the boundary of the gap continues its forward motion unimpeded. More clouds of plasma are seen filling the generated gap. The cusps are clearly seen, and clouds of plasma are also seen along the neutral line on the nightside. The magnetopause is still in its expansion phase at this stage, having a length of ~12.3 R_e from Earth along the x axis.

[30] In Figure 6b, taken at 1175 Δt, the subsolar magnetopause starts retreating earthward at around 43 R_e (Earth position is 60 R_e). We observe that the plasma flow enlarges the indentation at the cusp. On the other hand, the cusp region expands toward the poles. At this particular time, we clearly see an ~2-Re-thick belt/sheet of plasma formed at the dayside of the magnetopause; it appears at the nightside and has a thickness of about ~3 R_e. Here the dayside magnetopause structure never breaks as it did when $B_z = 0$. In Figure 6b, taken at 1250 Δt, the dayside magnetopause recovers its classical shape after the boundary of the gap passes over the planet. The effect of the reduction of the ram pressure can be felt at 63–80 R_e along Ox. We see that the cusp outflow region becomes more flared relative to the Earth-Sun line. At 100–140Δ, we observe that the tail boundary is reduced, thereby increasing the plasma sheet thickness. *Birn* [2005] discussed the relation between the tail boundary reductions and the plasma sheet thickness at the magnetotail, a relation that our simulation seems to confirm. The denser plasma comes from the nightside that feeds the equatorial plane along the neutral line.

[31] Figure 6a shows the field topology corresponding to the particle density in Figure 6a. The diffusion of the field lines with respect to the plasma at 15–30 R_e shows a drop in their strength because of the noticeable drop of the plasma dynamic pressure in that area. An opening of the field lines

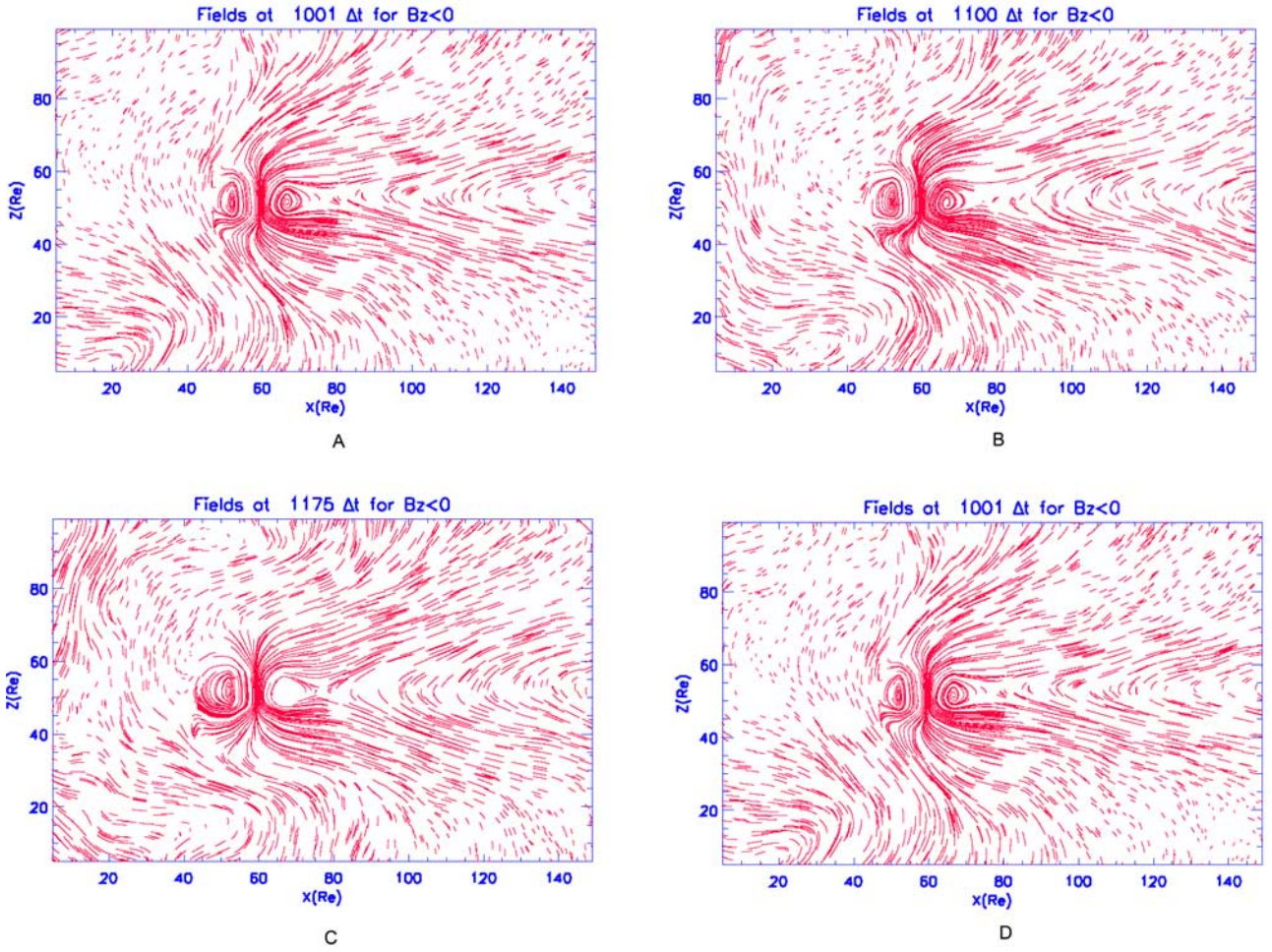

Figure 6b. Time sequence of the response of Earth's magnetosphere to a depression (air pocket effect) in the incident solar wind flow for $B_z < 0$. Field lines are shown in panels A, B, C and D, taken at 1001, 1100, 1175, and 1250 Δt, respectively. All plots are shown in the x-z plane located at $y = 52\ R_e$.

and the signature of reconnection are observed at the dayside magnetopause. This signature is seen better at (x, z) = (43, 37) R_e, when the image is zoomed between ($x = 5-80\ R_e$) and ($z = 25-90\ R_e$). The Earth's bow shock is seen at $\sim 42-46\ R_e$. At the upper and lower lobes of the magnetotail at points (x, z) = (100, 62) R_e and (100, 43) R_e, respectively, a fishtail shape configuration is observed. In addition, an x point formed at $\sim 80\ R_e$.

[32] In panel B, instabilities seen at $5-30\ R_e$ are due to the cumulated effects of the new, fast-approaching solar wind plasma as well as the plasma that slows down from the gap during 100 Δt. Indentations of the field intensities are seen ahead of the subsolar point and reflect the existence of the bow shock from 30 to 60 R_e. Enlargement of the dayside configuration of the magnetopause at the Sun-Earth line is seen at 46 R_e along x (Earth's position is 60 R_e). Field lines are driven tailward, and in this instance, an x point is observed at $\sim 80\ R_e$. The fishtail configuration appears with roughly the same position as the previous case. In panel C, as the upstream boundary of the plasma approaches the subsolar point, field lines become stronger, a sort of convection. The upstream of the air pocket effect now hits the expanded magnetopause at the distance of $\sim 42\ R_e$ (at 18 R_e from the planet). The expansion of the magnetopause along the south-north direction is seen in the field topology. Magnetic erosion takes place in which field lines are bent tailward rather than squeezed; as a result, they feed the tail with particles. An x point is seen at $\sim 80\ R_e$ on the nightside, and the instabilities seen in panel B move earthward. In Figure 6b, the magnetic field topology at the magnetopause restores its classical bullet-like shape after the induced gap boundaries pass over the planet position at 60 R_e. Field lines in the cusp region show inclination to the nightside direction: In other words, this system is highly dynamic even in a very short instance of time. The topology seen in this figure resembles the classical structure of the magnetosphere field representation. The fishtail configuration is now more flared out due to the air pocket effect at points (x, z) = (90, 70) R_e and (90, 42) R_e, respectively, up to the box boundary.

4. Analysis and Comments

[33] Now that we have presented the main changes that occur in the macrostructure of the Earth's magnetosphere in response to a pulse depression in the solar wind drift velocity both with and without IMF, we next attempt to

understand the time evolution of the system, focusing on the region along the Sun-Earth direction and taking care to estimate the time response of the magnetosphere in the expansion and recovery phases following the gap (air pocket effect) travel across the system. One of the outstanding results obtained so far in this study is that in the case without IMF, after an expansion phase necessary to respond to the drop of the dynamic pressure of the incoming solar wind, the outer boundary (nose) of the magnetopause breaks up with open magnetic field lines at a distance of $\sim$15.48 R_e from Earth. This result is confirmed from both the plasma density and the distribution of field lines (for example, Figure 5b). When we think of the magnetopause as an interface of equilibrium between two opposite magnetic and particle pressures, our results for the case with no IMF show that the magnetopause (MP) boundary is dragged far enough from its equilibrium position to lead it to break up. In addition, in contrast to the case when IMF was included, no apparent modification in the global field resists this inflation. Indeed, in our case, there is neither ionosphere-magnetosphere coupling nor flux tubes that transfer plasma from the upper ionosphere into the inner magnetosphere and, hence, no modification of the magnetic field strength.

[34] To better understand the expansion phase of the MP surface, in the following, we study the dynamics of the reversed clouds/blobs of plasma inside the generated gap. The blobs are defined as those ensembles of low-density plasmas that seem detached from the boundary gap downstream and that reverse direction against the stream. Here we adopted the analytical method of *Mishin* [1993] to calculate the different plasma pressures inside the gap and around its upstream and downstream sides. At an early stage of the process and downstream of the gap, one may sketch a simple scenario: The drop in the solar wind drift velocity from $V_1 = 0.25$ to $V_2 = 0.1$ induces a pressure gradient $\Delta P = \rho * ((V_2)^2 - (V_1)^2)$ that should drive a mechanical force $F = \Delta P/\Delta l$ oriented along the x axis, where Δl is a scale length that should be close to the width of the gap's edge. Because $\Delta P < 0$, this mechanical force is directed sunward and should accelerate particles back from the upstream of the magnetopause. As the flow has an initial bulk velocity directed opposite to the force direction, the induced force will stop the particles and then will reverse their velocity direction sunward (against the initial direction of the flow). The fascinating result is that the mechanical acceleration is so strong in the gap region that the plasma is blown off backward, sweeping the field lines away with it. This result is responsible for making the MP expansion run linearly along x, and later causing it to break up at a certain distance. By contrast, in the $B_z < 0$ case, such a mechanical process does not seem to dominate as the IMF should slow its impact. This is evidenced in our simulation as the magnetopause structure holds in the gap region when the IMF is present. One may sketch the following scenario: The mechanical force induced by the pressure drop accelerates the particles sunward, but the IMF field lines then play their role as a barrier. Indeed, for newly traveling-sunward particles of velocity v, a Lorentz force should deflect them, thus slowing their motion. As a result, one may expect a flattened, similar to the plane shape of the IMF barrier, but confined magnetopause interface that should not break up as is the case when IMF is absent.

[35] The question now becomes: Can we observe such a breakup of the magnetopause structure during the natural course of evolution of the Earth's magnetosphere? According to our case study, a few conditions are required. First, a strong depression should appear in the solar wind ram pressure. This is a rather usual situation as these events are common, and the event should last long enough that its dynamics has an impact on the magnetopause. Second, during the depression event, the IMF along z should be almost zero. With these ingredients, we predict that an expansion of the magnetopause size would lead to a breakup of its nose structure along the direction of depression of the solar wind. The main signatures of this breakup are sunward plasma motion and field lines opening. In our case, the air pocket volume is sketched with a planar cross section, but in nature, the volume of this depression could be much more confined and localized such that only the magnetosphere region, corresponding to the air pocket cross section across the flow axis that faces it, will be mostly affected. Additionally, in contrast to a reconnection event, the plasma is ejected from the magnetosphere cavity rather than injected.

[36] Until now, we have focused only on the magnetopause evolution from the Earth side. Other features could be observed when looking at the downstream boundary of the gap that defines the other edge of the plasma layer upstream of the magnetopause. As the gap travels earthward, the size of that plasma layer shrinks until it collapses and/or the second edge of the gap region is reached. The intriguing result is that the gap edge position measured from Earth does not fit with its natural motion but rather is slightly affected by plasma loss in an unexpected way. Indeed, during the period of the gap's travel across the magnetosphere, we observed that blobs of plasma detach from the downstream edge, shrinking (by mass loss) the size of the plasma layer between the gap and the magnetopause. To highlight this phenomenon, we generated a time sequence of the noon-midnight cross section of the Earth's magnetosphere at 1075, 1081, 1086, and 1091 Δt.

[37] For the sake of clarity, a region zoomed in between $10\Delta \leq x \leq 89\Delta$ and $30\Delta \leq z \leq 69\Delta$ was selected. As shown in Figure 7, and much like coronal mass ejections from the Sun, we see the formation of blobs of plasma (two are circled in the image) that are ejected into the gap space after a lapse of time. We believe that these unusual blobs are the consequence of the mutual impacts, respectively, of the depression force and the instability of the plasma layer that stands upstream in the magnetopause.

[38] Aside from the spectacular features reported above, in the following, we focus on the expansion/recovery phases of the magnetopause during the depression/compression of the solar wind dynamic pressure, taking care to estimate the relevant relaxation time.

[39] In Figure 8, panels A, B, and C represent the expansion/recovery phase when $B_z = 0$ and when they are measured through the size of the magnetopause along x (from Earth), y (dawn to dusk), and z (south to north), respectively. Here x represents the Sun-Earth line [at $(y, z) = (52, 53)$ R_e], y represents dawn-dusk line [at $(x, z) = (60, 53)$ R_e], and z represents south-north line [at $(x, y) = (60, 52)$ R_e]; no tilt is

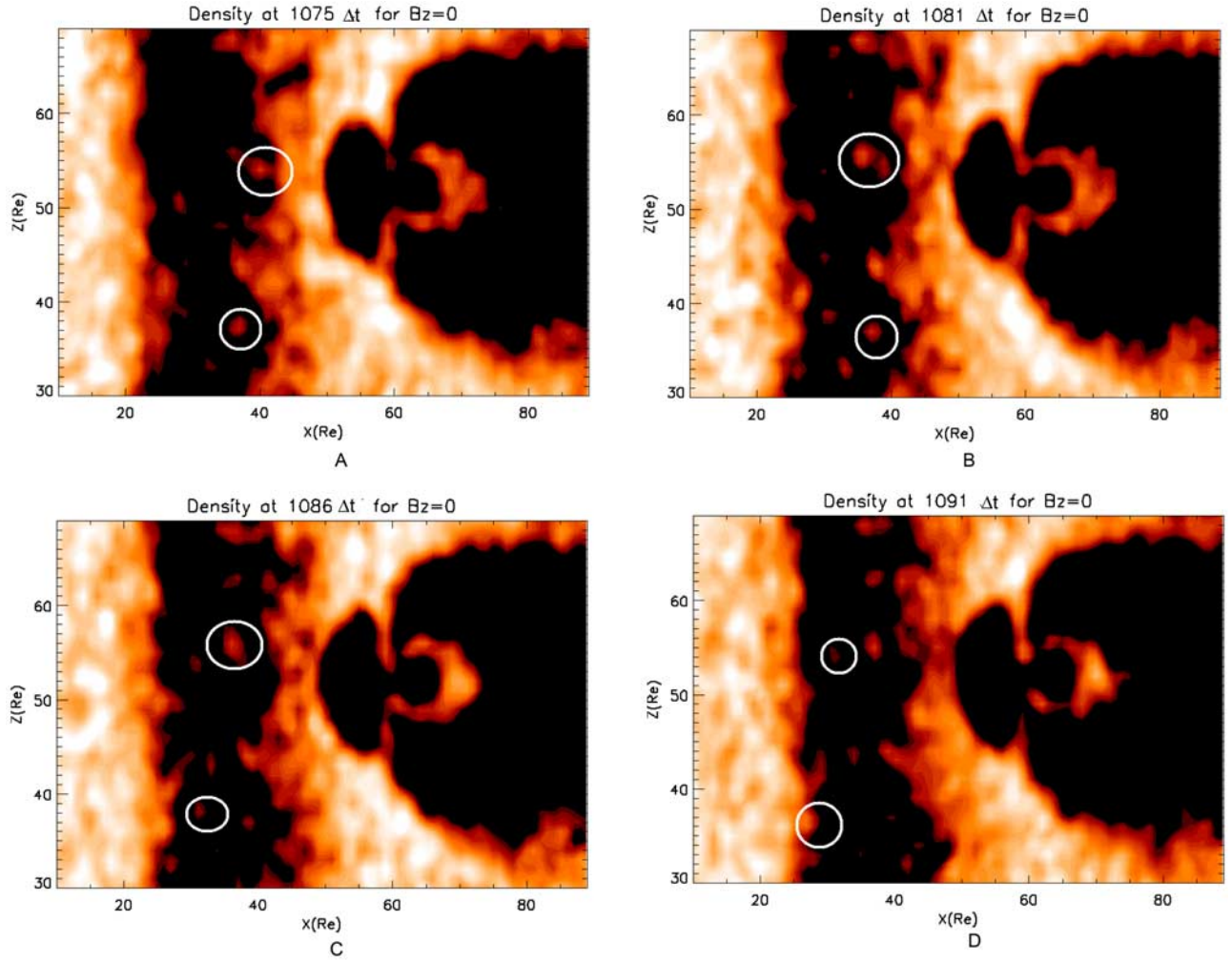

Figure 7. Time sequence of the detachment and sunward travel of a blob of plasma in the gap when no IMF is applied ($B_z = 0$). Plasma density is shown in panels A, B, C and D, taken at 1075, 1081, 1086, and 1091 Δt, respectively. All plots are shown in the x-z plane located at $y = 52\ R_e$ and zoomed in between $x = [10-89]\Delta$ and $z = [30-69]\Delta$. Images' contrast was increased to highlight the blobs.

assumed. To locate the magnetopause boundary along any axis, we plot the density profile and look for the abrupt drop-off of the density by definition of the stagnation region. Next, we measure the position of that density edge relative to the Earth's position at $(x, y, z) = (60, 52, 53)\ R_e$. Panels D, E, and F are the corresponding values in three-dimensional form when $B_z < 0$. In panel A, the magnetopause response to the abrupt change shows a nearly fast linear expansion of its size from ~10 up to ~15 R_e between 1117 and 1130 Δt. Since the gap (air pocket effect) extension is large enough, the induced nonrestricted force blows off the magnetopause structure and the magnetopause boundary breaks up at ~15.5 R_e at ~1132 Δt, leaving the magnetopause with an open boundary. As the upstream gap boundary moves closer to the new, expanded magnetopause, plasma accumulates and again produces enough dynamic pressure to balance the dipole magnetic one. It is interesting to note how that expansion phase (in terms of distance) grows faster than the recovery phase. By contrast, in the case when $B_z < 0$, as shown in Figure 8D, the magnetopause expands from 10 up to 18 R_e nonlinearly. Existence of B_z makes the expansion phase slower, thus leading to shorter distances of the MP for the same step time. In other words, the IMF confines the plasma, and the magnetopause never breaks up. This expansion takes place within duration between 1089 and 1072 Δt.

[40] In panel B, the magnetopause in y direction with $B_z = 0$ shows a different behavior. Its length expands from 17 up to 28 R_e, but between 1141 and 1198 Δt, the length relaxes for 4 Δt, and then the magnetopause shrinks back for ~2 R_e (probably due to induced pressure by the tiny particle ensembles inside the gap) and stays there until 1204 Δt. At 1204 Δt, the system again starts its expansion for ~4 R_e up to 1208 Δt. At this stage, the system enters the recovery phase and restores its average length of ~14 R_e at 1244 Δt. Yet in Figure 8E, where we have $B_z < 0$, the result is different. The expansion phase takes place very slowly between 1087 and 1205 Δt, and the recovery phase is very fast between 1205 and 1236 Δt. Now, in the expansion phase, the magnetopause size grows slowly and nonlinearly up to ~35 R_e until 1205 Δt. The recovery of the magnetopause size in the y direction takes place very quickly: It

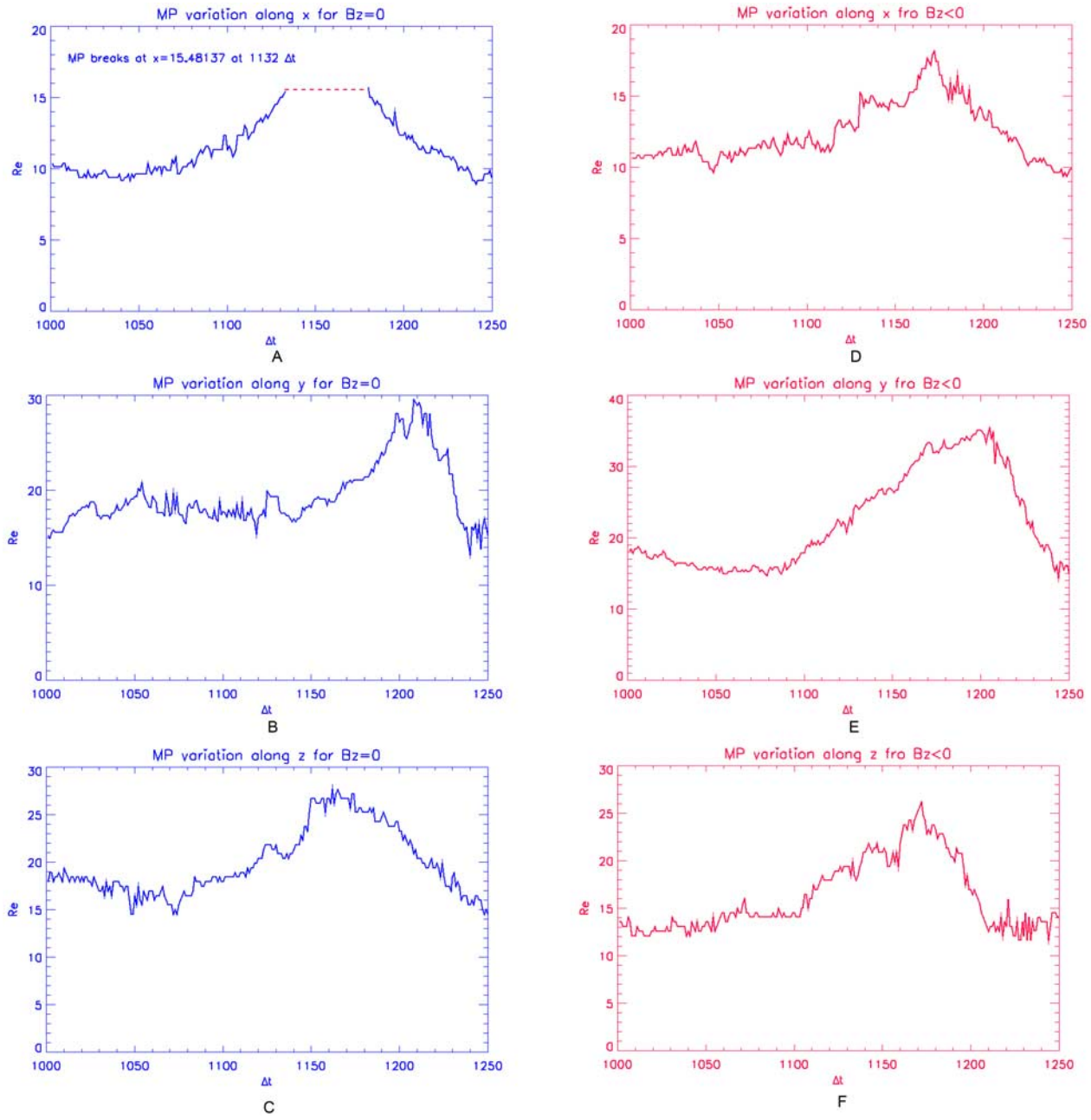

Figure 8. Magnetopause expansion/recovery measured from Earth location (x, y, z) = (60, 52, 53)R_e in three-dimensional form along x, y, and z axes for both $B_z = 0$ (panels, A, B, and C) and $B_z < 0$ (panels, D, E, and F), respectively. Panel A shows that during its expansion phase, the MP breaks down at a distance $\sim$15 R_e from Earth when zero IMF is applied.

shrinks from $\sim$35 to $\sim$16 R_e between 1205 and 1240 Δt. We believe that the fast recovery of the magnetopause is due to a magnetic force directed tailward (the slingshot effect) that adds to the magnetic force of the dipole when the dynamic pressure of the solar wind overpasses the magnetopause boundary for $B_z < 0$.

[41] Figure 8C, obtained similarly when $B_z = 0$, reveals that the expansion phase along z reaches $\sim$21 R_e between 1081 and 1124 Δt and then shrinks for 10 Δt for $\sim$1.4 R_e. It expands again to $\sim$27 R_e at 1162 Δt and recovers its initial value between 1162 and 1225 Δt. In panel F, when $B_z < 0$, we have a perturbed expansion of the size in z direction for $\sim$26 R_e between 1101 and 1172 Δt; the system then recovers its equilibrium position between 1172 and 1220 Δt. We measured the size of the magnetopause 5 R_e away from the vertical position of the dipole to avoid the interference of our readings with the cusp's position, a region that is highly susceptible to pressure gradients.

5. Discussion

[42] It may be useful at this stage to compare our results with existing studies and to assess their novelty in the rich

literature related to the solar wind interaction with the Earth's magnetosphere.

[43] Our simulation code is an updated version, in terms of numerical stability and computer CPU (resource usage), of an existing PIC EM particle code that has been used in the past to simulate the macrostructure of the Earth's magnetosphere [*Buneman*, 1993; *Nishikawa et al.*, 1995; *Wodnicka*, 2001]. However, in terms of boundary conditions, charge conservation, grid cells, and number of particles per cell, our code's version is similar to the one used by *Buneman* [1993], *Buneman et al.* [1995], *Villasenor and Buneman* [1992], *Nishikawa* [1997], *Nishikawa* [1998], *Nishikawa et al.* [1995], *Nishikawa and Ohtani* [2000], and *Cai et al.* [2003]. Recent work by *Cai et al.* [2006] improved the statistics of the code by using a higher density of particles per cell and a better resolution for the field description (0.5 R_e scale compared to 1 R_e in our case). It is out of the scope of this paper to go into a discussion of the numerical details of the PIC code, a description that is left to a forthcoming study (*L. Ben-Jaffel et al.*, in preparation, 2006).

[44] The novelty of the present work is to expand the use of the PIC code to simulate a drop in the dynamic pressure (depression) of the solar wind flow and to study the consequent time relaxation of the magnetosphere as it responds to the resulted disturbance for different orientations of the IMF. To the best of our knowledge, this is the first time a PIC code has been used for this kind of simulation. Our simulation for the depression of the solar wind pressure produced a planar volume of depletion in the plasma (Figures 4, 5a, and 6a), with sharp edges perpendicular to the x direction propagating earthward. In the real solar wind, an analogous depression in the IMF strength has been observed just upstream of the bow shock by three satellites AMPTE UKS, IRM, and ISEE1 [*Chisham et al.*, 2000]. In our PIC model, the solar wind pressure perturbation (gap), as it approaches the magnetosheath region, is decelerated with the generation of instabilities, evidenced both in the plasma distribution and in the field line topology, for both the zero and nonzero IMF cases (see (Figures 5a) and (6)]. Our results seem consistent with the general idea for the occurrence of instabilities and turbulence in the magnetosheath as observed by Cluster [*Lucek et al.*, 2005].

[45] In our study, in response to the depression of the solar wind pressure, the magnetopause expands along x direction from 10 out to 15 R_e with an average speed of 0.12 (solar wind drift velocity is 0.25) and then recovers with an average speed of 0.133 (equivalent to $\sim$266 km/s). We also note that if the perturbation is spatially confined, only a limited section of the magnetopause should expand.

[46] After we generated our simulation, we found a report on the observation by Interball-1 and Magion-4 of a hot flow anomaly (HFA) with a strong depression that allowed the magnetopause to expand sunward by as much as 5 R_e from its nominal position [*Sibeck et al.*, 1999]. According to *Sibeck et al.* [1999], the HFA was born after an IMF tangential discontinuity interacted with the Earth's bow shock. The results of our simulation are remarkably consistent with the Interball-1 observations. Thus hot flow anomalies are a class of discontinuities that can be handled by our simulation model. These results open new horizons for future work using this code to study the propagation of solar wind discontinuities and their impact on the magnetosheath/magnetopause system. In the past, these studies were usually conducted using MHD modeling [*Samsonov et al.*, 2006, and references within]. In the future, it would be useful to compare a PIC code simulation of the interaction of solar wind discontinuities with the Earth's magnetosphere to previous MHD calculations.

[47] During our study of time propagation of the depressed ram pressure of the solar wind, we noticed some penetration of solar wind plasma into the magnetospheric cavity. Despite the fact that our code was run with a relatively large spatial scale (1 R_e) for the fields, many other dynamic processes were observed around the magnetopause boundary. These processes were the candidate processes responsible for the penetration of solar wind particles into the inner Earth magnetosphere, based on CLUSTER observations presented in the work of *Phan et al.* [2005]. As an example, our simulation showed that one can track up to two x points in the magnetotail neutral sheet as indicated by two arrows in Figure 5b. These results are remarkably consistent with Cluster report of multiple x-line structure in the Earth's magnetotail current sheet [*Eastwood et al.*, 2005]. Future quantitative comparison of our simulation to Cluster data will surely be very useful to understand the processes at the origin of the observed multiple x points.

6. Summary and Concluding Remarks

[48] In this paper, a new approach is used to study the sensitivity of the Earth's magnetosphere to the variability of the solar wind bulk velocity. We use a three-dimensional electromagnetic PIC code as the technical tool to achieve our work (*L. Ben-Jaffel et al.*, in preparation, 2006) and reach the following conclusions:

[49] The code was tested with different grid sizes and solar wind input parameters. In all cases, the formation of the magnetospheric cavity and its elongation around the planet were observed. The expected classical macrostructure of the magnetosphere was obtained.

[50] A single test case of depression/compression was carried out to simulate the highly variable nature of the solar wind. As a result, an "air pocket," or gap, was noticed, with the expected size and position.

[51] Low-density plasma inside the generated air pocket reversed direction at an early time when $B_z = 0$ but continued flowing along the stream when $B_z < 0$ with more density fillings.

[52] Magnetopause dayside boundary broke up during the sunward expansion phase when $B_z = 0$, but it sustained its shape when $B_z < 0$.

[53] Blobs of plasma get detached from the downstream edge of the gap, reducing by mass loss the width of the plasma layer that sustains the magnetopause.

[54] Orientation of the cusps is highly affected by the depression in the solar wind flow. Lobes flared out when $B_z = 0$ due to the air pocket effect.

[55] Indication of reconnection is observed for $B_z < 0$ through the manifestation of particles injected inside the inner magnetosphere.

[56] When $B_z = 0$, the magnetopause expanded and recovered linearly in x direction. When $B_z < 0$, the processes of expansion and recovery were not linear.

[57] x point was found at around 103 R_e for $B_z = 0$, while it read ~80 R_e for $B_z < 0$. The gap (air pocket) size formed was ~15 R_e for both $B_z = 0$ and < 0.

[58] Earth's bow shock was successfully simulated and was shown for both plasmas and fields.

[59] Quick comparison to existing observations from Cluster, Interball-1, and Magion-4 satellites seems to confirm many of our simulation results, particularly regarding the fast sunward expansion of the magnetopause in response to a strong drop in the solar wind pressure.

[60] **Acknowledgments.** The authors acknowledge very helpful discussions with E. Wodnicka, B. Popielawska, and Jolanta Grygorczuk from Space Research Center (Poland). L. Ben-Jaffel acknowledges support from Centre National d'Etudes Spatiales of France, CNES, under Project Inspire.

[61] Zuyin Pu thanks the reviewers for their assistance in evaluating this paper.

References

Balogh, A., C. M. Carr, M. H. Acuna, et al. (2001), The Cluster magnetic field investigation: Overview of in-flight performance and initial results, *Ann. Geophys.*, *19*, 1207.

Bauer, T. M., M. W. Dunlop, B. U. O. Sonnerup, N. Sckopke, A. N. Fazakerley, and A. V. Khrabrov (2000), Dual spacecraft determinations of magnetopause motion, *Geophys. Res. Lett.*, *27*, 1835.

Birn, J. (2005), Three dimensional magnetotail equilibria with prescribed boundary shapes, *J. Geophys. Res.*, *110*, A07203, doi:10.1029/2004JA010869.

Boris, J. P. (1970), Relativistic plasma simulation optimization of a hybrid code, paper presented at 4th Conference on Numerical Simulation of Plasmas, Naval Res. Lab., Washington, pp. 3–67, 2–3 November.

Buneman, O. (1993), TRISTAN, in *Computer Space Plasma Physics: Simulation Techniques and Software*, edited by H. Matsumo and Y. Omura, pp. 67–84, Terra Sci., Tokyo.

Buneman, O., K.-I. Nishikawa, and T. Neubert (1995), Solar wind-magnetosphere interaction as simulated by a 3D EM particle code, in *Space Plasmas: Coupling Between Small and Medium Scale Processes*, *Geophys. Monogr. Ser., 86*, edited by M. Ashour-Abdullah, T. Chang, and P. Duenburg, pp. 347–352, AGU, Washington, D. C.

Burch, J. L. (2005), Magnetospheric imaging: Promise to reality, *Rev. Geophys.*, *43*, RG3001, doi:10.1029/2004RG000160.

Cai, D., X. Y. Yan, K.-I. Nishikawa, and B. Lambege (2006), Particle entry into inner magnetosphere during duskward IMF B_y: Global three-dimensional electromagnetic full particle simulations, *Geophys. Res. Lett.*, *33*, L12101, doi:10.1029/2005GL023520.

Cai, D., L. Yaoting, N. Ken-Itchi, X. Chiji, Y. Xiaoyang, and P. Zuying (2003), Parallel 3-D electromagnetic particle code using high performance FORTRAN: Parallel TRISTAN, in *Space Plasma Simulation*, edited by J. Büchner, C. Dum, and M. Scholer, *Lect. Notes Phys., 615*, pp. 25–53.

Chisham, G., S. J. Schwartz, D. Burgess, S. D. Bale, M. W. Dunlop, and C. T. Russell (2000), Multisatellite observations of large magnetic depressions in the solar wind, *J. Geophys. Res.*, *105*(A2), 2325–2336.

Eastwood, J. P., D. G. Sibeck, J. A. Slavin, M. L. Goldstein, B. Lavraud, M. Sitnov, S. Imber, A. Balogh, E. A. Lucek, and I. Dandouras (2005), Observation of multiple X-line structure in the Earth's magnetotail current sheet: A Cluster case study, *Geophys. Res. Lett.*, *32*, L11105, doi:10.1029/2005GL022509.

Escoubet, C. P., and R. Schmidt (2000), Cluster II: Plasma measurements in three dimensions, *Adv. Space Res.*, *25*(7–8), 1305–1314.

Guzdar, P. N., X. Shao, C. C. Goodrich, K. Papadopoulos, M. J. Wiltberger, and J. G. Lyon (2001), Three-dimensional MHD simulations of the steady state magnetosphere with northward interplanetary magnetic field, *J. Geophys. Res.*, *106*(A1), 275–288.

Haaland, S. E., et al. (2004), Four-spacecraft determination of magnetopause orientation, motion and thickness: Comparison with results from single-spacecraft methods, *Ann. Geophys.*, *22*, 1347–1365.

Hasegawa, H., M. Fujimoto, K. Takagi, Y. Saito, T. Mukai, and H. Rème (2006), Single-spacecraft detection of rolled-up Kelvin-Helmholtz vortices at the flank magnetopause, *J. Geophys. Res.*, *111*(A9), A09203, doi:10.1029/2006JA011728.

Lindman, E. L. (1975), Free-space boundary conditions for the time dependent wave equation, *J. Comput. Phys.*, *18*, 66–78.

Lucek, E. A., D. Constantinescu, M. L. Goldstein, J. Pickett, J. L. Pinçon, F. Sahraoui, et al. (2005), The magnetosheath, *Space Sci. Rev.*, *118*(1-4), 95–152.

Lyon, J. G., R. E. Lopez, C. Goodrich, M. Wiltberger, and K. Papadopoulos (1998), Simulation of the March 9, 1995, sub-storm: Auroral brightening and the onset of lobe reconnection, *Geophys. Res. Lett.*, *25*, 3039.

Matsumoto, H., and Y. Omura (1993), *Computer Space Plasma Physics, Simulation Techniques and Software*, Terra Sci., Tokyo.

Mishin, V. V. (1993), Accelerated motions of the magnetopause as a trigger of the Kelvin-Helmholtz instability, *J. Geophys. Res.*, *98*, 21,365–21,371.

Murr, D. L. (2004), Scarf award presentation: Magnetosphere-ionosphere coupling studies of dayside high-latitude transients, *Eos Trans. AGU, 85*(47), Fall Meet. Suppl., Abstract SM41B-01.

Nishikawa, K. I. (1997), Particle entry into the magnetosphere with a southward interplanetary magnetic field studied by a three-dimensional electromagnetic particle code, *J. Geophys. Res.*, *A8*, 17,631–17,641.

Nishikawa, K. I. (1998), Particle entry though reconnection grooves in the magnetopause with a dawnward IMF as simulated by a 3-D EM particle code, *Geophys. Res. Lett.*, *25*(10), 1609–1612.

Nishikawa, K. I., and S. Ohtani (2000), Evolution of thin current sheet with a southward interplanetary magnetic field studied by a three-dimensional electromagnetic particle code, *J. Geophys. Res.*, *105*(A6), 13,017–13,028.

Nishikawa, K. I., T. Neubert, and O. Buneman (1995), Solar wind-magnetosphere interaction as simulated by a 3-D EM particle code, *Astrophys. Space Sci.*, *227*, 265–276.

Phan, T. D., C. P. Escoubet, L. Rezeau, R. A. Treuman, A. Vaivads, G. Paschmann, S. A. Fuselier, D. Attié, B. Rogers, and B. U. O. Sonnerup (2005), Magnetopause processes, *Space Sci. Rev.*, *118*, 367–424.

Reiff, P. H., and J. L. Burch (1985), IMF By-dependent plasma flow and Birkland currents in the dayside magnetosphere: 2. A global model for northward and southward IMF, *J. Geophys. Res.*, *90*, 1595.

Samsonov, A. A., Z. Němeček, and J. Šafránková (2006), Numerical MHD modeling of propagation of interplanetary shocks through the magnetosheat, *J. Geophys. Res.*, *111*(A8), A08210, doi:10.1029/2005ja011537.

Sibeck, D. G., N. L. Borodkova, S. J. Schwartz, et al. (1999), Comprehensive study of the magnetospheric response to the hot flow anomaly, *J. Geophys. Res.*, *104*, 4577–4594.

Villasenor, J., and O. Buneman (1992), Rigorous charge conversation for local electromagnetic field solvers, *Comput. Phys. Commun.*, *69*(2-3), 306–316.

Winglee, R. M., W. Lewis, and G. Lu (2005), Mapping of the heavy ion outflows as seen by IMAGE and multi-fluid global modeling for the 17 April 2002 storm, *J. Geophys. Res.*, *110*, A12S24, doi:10.1029/2004JA010909.

Wodnicka, E. B. (2001), Comparing two models of the Earth's magnetosphere, *Adv. Space Res.*, *28*(12), 1727–1732.

S. Baraka and L. Ben-Jaffel, Institut d'Astrophysique de Paris, UMR7095 CNRS, Université Pierre et Marie Curie, 98 bis Boulevard Arago, 75014 Paris, France. (baraka@iap.fr)